Lab on a Chip

Accepted Manuscript

ROYAL SOCIETY OF CHEMISTRY

www.rsc.org/loc

Journal Name

RSCPublishing

ARTICLE

Efficient coupling of acoustic modes in microfluidic channel devices

Cite this: DOI: 10.1039/x0xx00000x

M. Bora*, and M. Shusteff

Received ooth January 2012,
Accepted ooth January 2012

DOI: 10.1039/x0xx00000x

www.rsc.org/

This work introduces a new numerical simulation approach to acoustic microfluidic chip design based on coupled-resonator theory. A simplified acoustofluidic device operating in the transverse elastic mode is investigated and optimized for maximal pressure standing wave amplitude. This design approach provides insights into the symmetry and frequency characteristics of acoustic chip resonances that cannot be obtained from analysis based on wave propagation arguments. The new approach reveals that optimal performance requires spatial symmetry-matching and frequency-matching of the full device's elastic resonance to the channel's acoustic resonance. Symmetry selection is demonstrated for a three terminal piezoelectric transducer actuation scheme showing suppression of opposite-symmetry and enhancement of same-symmetry acoustic modes. Excitation of ultrasonic waves exhibits the anti-crossing behaviour predicted by coupled mode theory with acoustic mode splitting into two distinct branches. Increased efficiency of energy transfer from the transducer into the fluid, with its corresponding increase in pressure amplitude suggests a potential path toward significant increases in acoustic separator performance.

Introduction

Lab on a chip devices aim to transfer the functionality of common laboratory tasks to a miniaturized chip-based footprint with significant advantages expected in handled fluid volumes, implementation speed, and cost savings. Particle sorting and separation are an important category of these tasks, and rely on a variety of fluidic, magnetic, optical, electrical, and other approaches[1, 2]. Acoustic particle manipulation in microfluidic devices has gained in prevalence dramatically, with over a hundred peer-reviewed journal citations in 2014 alone, exceeding the aggregate number over all the years prior to 2008. Acoustic separation is based on excitation of ultrasonic standing waves in fluid channels, producing a radiation force field that moves particles to the pressure nodes of a standing wave pattern[3, 4]. However, an important limitation of acoustofluidic devices is the large power input required (~1-10 W), implying low-efficiency transfer of energy into the fluid that is available for particle handling. This constrains the utility of acoustics devices, for example making deployment in low-resource settings impractical. We hypothesize that the coupling between the piezoelectric actuator and the microfluidic chip is one of the key design parameters that may be optimized for significant gains in device efficiency. In this work we study the achievable improvements in acoustic efficiency using an approach to acoustofluidic resonator design based on finite-element modelling of the structure's elastic behaviour.

Common acoustofluidic devices consist of a voltage actuated piezoelectric transducer that converts electrical to mechanical energy[5], coupled to a chip with a microfluidic channel. In bulk acoustic wave (BAW) devices, ultrasound propagates throughout the multilayer structure, and the fluid channel acts as an acoustic resonator that is excited via elastic deformations normal to its walls[6]. In a first order approximation, acoustic fluid cavity width is a multiple of sound half-wavelengths, with second order corrections accounting for viscous losses and non-ideal boundary conditions[7]. In surface acoustic wave (SAW) devices[8, 9], ultrasound energy propagates along surfaces, coupling evanescently into the fluid, and channels are commonly made of lossy elastomer (e.g., PDMS), resulting in lower efficiency compared with BAW devices. It is therefore most valuable to consider optimizing BAW-type acoustic devices to attain maximally efficient acoustic particle manipulation.

The primary radiation force (PRF) acting on a spherical particle in an ultrasound pressure field has been calculated for both ideal[10, 11] and viscous[12] fluids. The force arises from the gradient of the acoustic potential, which, for a spherical particle can be approximated by:

$$U = \frac{V}{2}\left(\kappa_f - \kappa_p\right)\left\langle p^2 \right\rangle \quad (1)$$

Where V is the particle volume, κ_f and κ_p, the compressibility of fluid or particle, p, pressure and brackets indicate time average. These calculations indicate that, among other factors, the PRF is proportional to the square of the pressure amplitude. Effective acoustic sorting therefore requires maximizing the pressure amplitude in the resonant fluid cavity; thus, we will use the pressure amplitude as a key figure of merit in much of the following discussion.

A range of device architectures have been proposed, including cylindrically symmetric configurations for capillary acoustophoresis[13-15] or layered chips comprising the ultrasonic coupler, fluid layer and reflector in both horizontal[16] ("layered resonator") and vertical[17, 18] ("transversal resonator") configurations. The latter approach has the benefit of employing standard microfabrication processing, with channels etched in silicon and bonded to glass for optical access. In these devices the acoustic standing wave is perpendicular to the piezoelectric actuation direction[19] and proposed optimal configurations suggest lateral distances between channel walls and chip edges of odd multiples of quarter sound wavelengths[20]. Because of the widespread adoption of the transversal resonator, this work is focused on this format.

Piezoelectric transducer geometry plays an important role in the type of excited acoustic modes. Configurations of the piezo electrodes as thin side strips, and half-width, and full-width sections result not only in distinct pressure amplitudes but also in different modes[21]. Alternative approaches replace piezoelectric plates with a wedge-shaped transducer, reporting optimal wedge angle of 30 degrees, and advantageous asymmetric transducer placement[22].

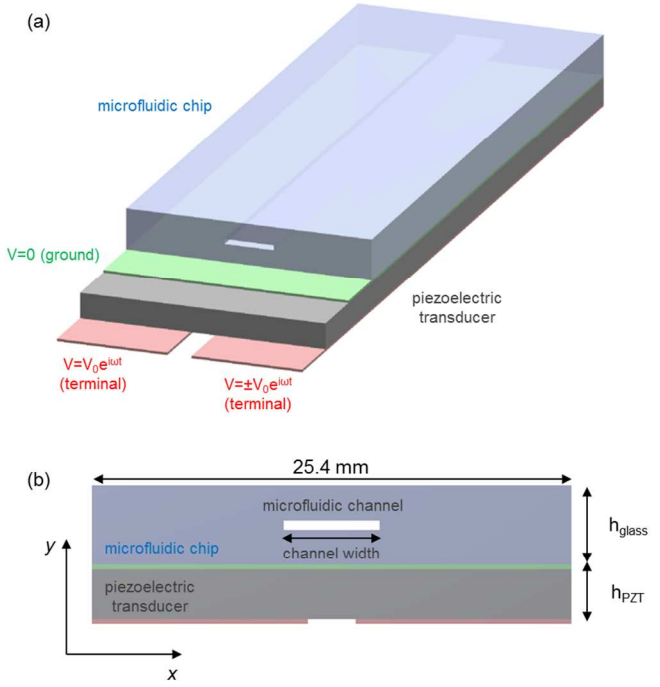

Fig. 1 (a) Design of acoustofluidic device consisting of piezoelectric transducer, microfluidic chip and acoustic channel. A three electrode voltage actuation of the piezoelectric transducer enables selection of acoustic modes of defined symmetry when the voltage on the two red terminals is in phase (Δϕ=0, symmetric) or in opposite phase (Δϕ=π, antisymmetric). (b) Cross sectional view of the device with axis orientation and relevant dimensions.

In this work we undertake a numerical study using finite-element analysis of an acoustofluidic device design consisting of an all-glass chip bonded to a piezo transducer actuated in a three terminal configuration (Figure 1).

The proposed device operates at elastic transverse deformations in a configuration optimized for odd or even order acoustic modes. Maximum pressure amplitude is demonstrated for full-device thicknesses (piezoelectric and chip) that have transverse elastic frequency equal to that of the acoustic channel. The three-terminal actuation allows for excitation of elastic modes with specific symmetry, and we show the crucial role played by resonant mode symmetry.

Although most acoustofluidic devices are made in both silicon and glass, the device used in this work is all-glass, to reduce analytical complexity. Previous reports have demonstrated ultrasonic separators made entirely of glass,[23]. As an alternative to hydrofluoric acid wet etching, a number of studies report highly anisotropic vertical etching of glass using high energy femtosecond laser activation[24, 25], a technique already commercially available for high resolution three dimensional microfluidic chips.

This paper is organized as follows: first, we briefly review coupled resonator theory to motivate two major design rules. Then, we begin to build up the acoustofluidic device, by first analysing the resonant behaviour of each material separately: water, glass, and piezoceramic. Next, we examine the joined piezo-glass structure, (without a fluid channel) from a displacement-amplitude viewpoint. Finally the fluid channel is added to complete the analysis, identifying frequency and dimensional parameter combinations that maximize fluid pressure amplitude.

Theoretical background: coupled mode theory

The numerical simulations performed in this study rely on coupled mode theory to investigate the interaction between the chip components: microfluidic channel, solid chip substrate and piezoelectric driver. Briefly, the interaction between two interacting resonating systems (the glass-piezo structure, and the water cavity) can be described by the equations of motion for their generalized coordinates q_1 and q_2:

$$\begin{aligned} \dot{q}_1 - i\omega_1 q_1 - ikq_2 &= 0 \\ \dot{q}_2 - i\omega_2 q_2 - ikq_1 &= 0 \end{aligned} \quad (2)$$

The generalized coordinates q stand for any physical quantity describing the system (i.e. pressure for acoustics, displacement for elasticity and potential for piezoelectricity)[26, 27]. The resonant frequencies for each system are labelled as ω_1 and ω_2, and k represents the coupling constant between the two

resonators. Assuming harmonic solutions the coupled eigen-frequencies are given by setting the determinant of the equation system to 0:

$$\det\begin{pmatrix} \omega-\omega_1 & -k \\ -k & \omega-\omega_2 \end{pmatrix}=0 \quad (3)$$

with solutions that have the form:

$$\omega^{A,S}=\frac{\omega_1+\omega_2}{2}\pm\sqrt{\left(\frac{\omega_1-\omega_2}{2}\right)^2+k^2} \quad (4)$$

where the superscript *A*, *S* in equation (4) indicates the anti-symmetric and symmetric solutions. In Figure 2 the two solutions are plotted as a function of the second oscillator frequency with the frequency of the first oscillator being kept constant at ω_1. At the crossover point ($\omega_2=\omega_1$), the solutions split into two branches given by equation (4).

The most efficient coupling between the resonators occurs when the two frequencies are identical[28], and this leads to the first rule regarding acoustofluidic design: given a resonant frequency of the fluid channel, the combined piezo-glass mechanical structure has to resonate at that same frequency.

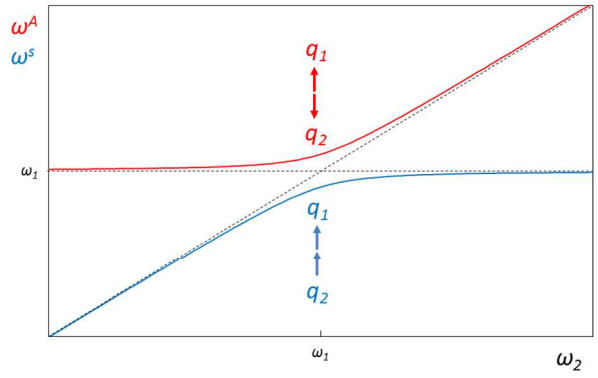

Fig. 2 Frequency crossing of two coupled oscillators, highlighting the anti-symmetric (red) and symmetric (blue) branches as a function of detuning between the two resonators. The frequency of the first resonator ω_1 is constant while the frequency of the second resonator ω_2 is varied.

Considering in addition the spatial symmetry of the two modes, they can be classified as either symmetric or anti-symmetric with respect to positional coordinate mirror mapping of *x* to *–x*:

$$q_{s(-x)}=q_{s(x)},\quad symmetry$$
$$q_{a(-x)}=-q_{a(x)},\quad antisymmetry \quad (5)$$

It is important to distinguish between the symmetries of oscillator coupling that specifies in phase (S), or out of phase (A) oscillation of the couple oscillators, labelled with capitalized superscripts, and the positional symmetry that describes each resonator mode's coordinate dependence, which is labelled as a lowercase subscript.

If the coordinate mirroring in equation (5) is introduced in equation (2), it is straightforward to notice that modes with distinct spatial symmetry are orthogonal to each other and have a null coupling coefficient *k*, introducing the second design rule for the acoustofluidic chip: given a coordinate symmetry of the acoustic mode in the channel, the chip-transducer system has to match it.

The optimal coupling of acoustic waves will follow the two rules mentioned earlier and are sufficiently general to be independent on how the coupling occurs or what the particular mode profile is for any of the components. In the following modelling section we will focus on identifying the simplest acoustofluidic device design that complies with these rules.

Modelling of acoustofluidic devices

Numerical modelling (COMSOL Multiphysics, Burlington, MA) is used to determine the resonant modes of the fluid channel, the elastic behaviour of the chip solid substrate, the piezoelectric modes of the acoustic transducer, and the mechanical interaction between each of the individual components of the acoustofluidic device.

Resonant modes for the rectangular cross section of the microfluidic channel

The resonant modes of a fluid channel are calculated using an eigenfrequency analysis by solving the wave equation for pressure:

$$\nabla^2 p-\left(\frac{\omega}{c}\right)^2 p=0 \quad (6)$$

with *p*, the acoustic pressure, $\rho=998\ kg/m^3$, the fluid density, $c=1481.4\ m/s$, the speed of sound in fluid and ω, the frequency. The boundary conditions at all four channel walls are initially set as sound hard or perfect reflector:

$$n\cdot\nabla p=0 \quad (7)$$

where *n* is the normal to the boundary.

The modes can be labelled by their index along the two axis (n_x, n_y) and were calculated for channels 100um high and 375 μm wide for the first and second resonant modes, respectively. The channel dimensions were chosen such that for the frequency range considered in this study only lateral modes are excited (i.e. $n_y=0$). Figure 3, (a) and (b) show the maximum normalized pressure distribution as a function of position for *(1, 0)* and *(2, 0)* modes with ultrasonic frequency of approximately 1.99 MHz and 3.98 MHz.

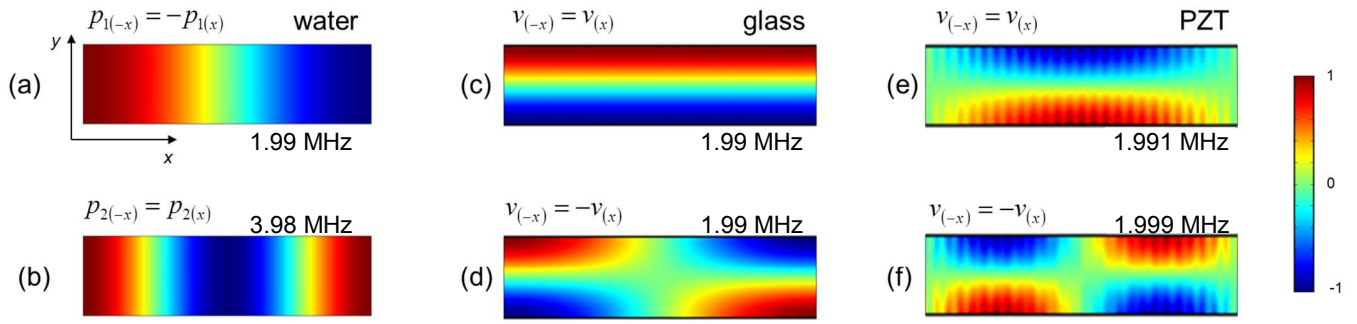

Fig. 3 Eigenmodes and symmetry relations for individual components of the acoustofluidic chip. Pressure amplitude profile for the first (a), and second order mode (b) for the rectangular cross section of a water-filled microfluidic channel along with the spatial symmetry relation for pressure (width 375 μm). Transverse resonant modes for maximum normalized vertical displacement *v* for a rectangular chip cross section in fused silica (25.4 by 1.5 mm, not to scale), highlighting the positional symmetry of the two modes (c) and (d). Resonant modes for the piezoelectric transducer (25.4 by 1.035 mm cross section) highlighting the maximum normalized displacement and coordinate symmetry with respect to the horizontal coordinate mirror transformation. Axis orientation in (a) is the same for all figures in this study.

The acoustic resonant modes have alternate coordinate symmetry dependent on the length of the channel being an odd or even multiple of sound wavelengths. Without loss of generality we will only consider the first two orders, but the present analysis can be extended to any mode of arbitrary order.

Resonant modes for the rectangular cross section of the glass chip

For the analysis that follows, the microfluidic chip is assumed to be made of fused silica with a rectangular cross-section, representative of chips fabricated by wafer bonding techniques. Although in many numerical studies of acoustofluidic devices, the analysis is done from an acoustic wave propagation perspective, a more complete description requires elastic modelling of the chip. While these two approaches generally lead to similar results, the elastic mode has the advantage of taking into account the role of the free chip edges, fluidic channel cut out, and to explore non-propagating elastic solutions. The fused silica is modelled as an isotropic linear elastic material of density $\rho=2203kg/m^3$ and Young modulus $E=73.1GPa$, and Poisson ratio $\upsilon=0.17$ using the tensor formulation of Hook's law:

$$\varepsilon = \frac{1}{2}\left(\nabla u + \nabla u^T\right)$$
$$s = C : \varepsilon \qquad (8)$$

with u, the displacement vector, ε, the strain tensor, s, the stress tensor, and C, the elasticity tensor with components derived from Young modulus and Poisson ratio values. An isotropic loss factor of 1% is added to the material elastic properties, estimated from the vendor-specified mechanical quality factor of 80 for the PZT material.

Elastic modes in the glass or piezoelectric material can be labelled using order index along the ***x*** and ***y*** axis (n_x, n_y) in a fashion similar to indexing of acoustic pressure modes[29]. Further, the modes are further distinguished as purely lateral, $(n_x, 0)$, or purely transverse, $(0, n_y)$. In our study, the length along ***x*** axis is much larger than the length along the ***y*** axis such that lateral resonances are attenuated more and have a weak effect on efficient excitation of acoustic modes. For the purposes of this discussion we define lateral modes as $(n_x, 0)$ and transverse modes as $(n_x, n_y\neq0)$.

The lateral size of the chip is 1 inch (25.4 mm) since this is a common dimension for microscope slides and many commercial suppliers provide devices with this width. Our results indicate that this dimension does not have a strong effect on the chip transverse elastic modes when the chip width is at least an order of magnitude larger than its height, mainly because in the MHz frequency range lateral modes have a longer and higher loss propagation length. The thickness of the chip was adjusted such that the relevant modes match the channel acoustic frequencies. Figure 3, panels (c) and (d), identify two transversely resonant modes for a rectangular cross section of a fused silica block of height 1.5 mm and width 25.4 mm. In this calculation only, the lateral modes are suppressed for clarity by constraining deformation along the vertical at the side boundaries. The values for the resonant frequencies found by eigenfrequency analysis are approximately 1.99 MHz, with a separation of ~3 kHz.

Resonant modes for the rectangular cross section of the piezoelectric driver

The piezoelectric element is used to excite elastic modes in the chip glass substrate that in turn will excite acoustic waves in the channel. We investigate transverse piezoelectric modes of defined symmetry due to their having high piezoelectric coupling coefficient and low losses.

The piezoelectric driver is modelled as a transversely anisotropic material based on properties of PZT-5A, with its anisotropy axis aligned with the vertical axis of the fluid channel cross section.

The eigenfrequency modes are calculated from the Poisson equation for the electric field E:

$$E = -\nabla V \qquad (9)$$

with V, the electric potential, and from piezoelectric effect coupling equation written in the stress charge form relating the stress, strain and electric field:

$$s = c_E : \varepsilon - e^T E \tag{10}$$

with s, the stress tensor, ε, the strain tensor calculated in the same way as in equation (8), c_E, the elasticity tensor for constant electric field, and e the coupling matrix for constant strain. As with the glass layer, an isotropic elastic loss of 1% is included in the model.

Numerical values for elasticity and coupling matrices are taken from the material data sheet for a piezo material we use in our acoustofluidic devices (PSI-5A4E, Piezo Systems, Woburn, MA) with the following matrix elements written in the Voight notation:

$$c_E = \begin{pmatrix} 152 & 102 & 100 & 0 & 0 & 0 \\ 102 & 152 & 100 & 0 & 0 & 0 \\ 100 & 100 & 127 & 0 & 0 & 0 \\ 0 & 0 & 0 & 21 & 0 & 0 \\ 0 & 0 & 0 & 0 & 21 & 0 \\ 0 & 0 & 0 & 0 & 0 & 25 \end{pmatrix} GPa$$

$$e = \begin{pmatrix} 0 & 0 & 0 & 0 & 12.4 & 0 \\ 0 & 0 & 0 & 12.4 & 0 & 0 \\ -5.5 & -5.5 & 16.4 & 0 & 0 & 0 \end{pmatrix} \frac{C}{m^2} \tag{11}$$

The piezoelectric transducer element width is set to be the same as the glass chip at 25.4 mm, and the thickness is adjusted to 1.035 mm, such that the free transverse resonant mode is approximately 1.991 MHz (symmetric) and 1.999 MHz (antisymmetric).

As in the glass chip mode analysis we look for transverse modes that are symmetric or antisymmetric. For this case the boundary conditions are mechanically free, with zero charge for the lateral sides of the PZT transducer. Figure 3, panels (e) and (f), show the symmetric and antisymmetric modes for the PZT transducer.

In practise selection of symmetric and antisymmetric modes can be achieved by placement of the piezoelectric transducer with respect to centre axis of the chip[22]. If the two are aligned only the symmetric mode is excited. If the piezoelectric element is offset from the centre then both modes are accessible. We propose a design based on a three terminal driver with one side grounded and the opposing face divided equally between two electrodes with a small separation of 0.5 mm between them. This design enables specific selection of either mode depending on the applied voltages. For example if both halves of the divided electrode are driven by the same voltage (+V and +V) only the symmetric mode is excited. If the electrodes are driven out of phase (i.e. +V and –V) only the antisymmetric mode is excited.

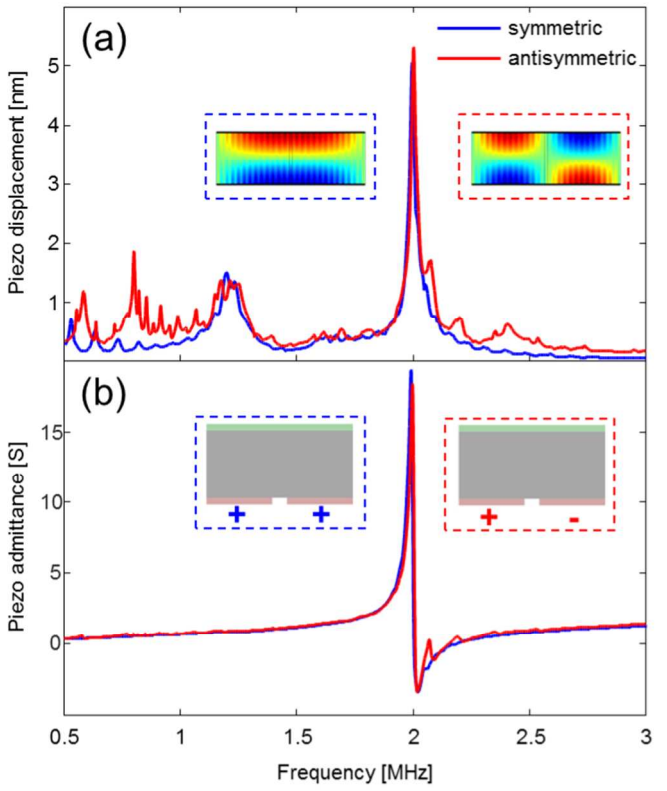

Fig. 4 Displacement amplitude (a) and admittance (b) as a function of excitation frequency for a three-terminal piezoelectric transducer designed for selective excitation of symmetric and antisymmetric modes. Elastic mode and drive configuration are shown in the insets.

This effect is demonstrated by simulating the admittance spectrum as a function of drive frequency. The electrical admittance is commonly measured to identify the resonances of piezoelectric transducers. In Figure 4 the admittance spectrum for both configurations is shown with the indication of both excited mode and drive conditions.

Piezoelectric transducer coupling to elastic modes in the chip

Elastic coupling between the PZT transducer and the chip is calculated by performing a quantitative analysis of coupled oscillation of transversal elastic modes.

A fully-developed model must account for the physical connection between the PZT and glass chip. However, because piezo attachment strategies vary widely, from ultrasonic gels to epoxies, modelling a particular configuration is of limited value. Therefore, to maintain the generality of this approach, and to represent a "best-case" scenario, in the following discussion we assume a perfectly bonded transducer-chip interface. We use continuity equations for displacement at the interface, under the assumption that this represents the strongest achievable bond. A study of adhesive materials, thickness and elastic parameters is an important topic for further investigation.

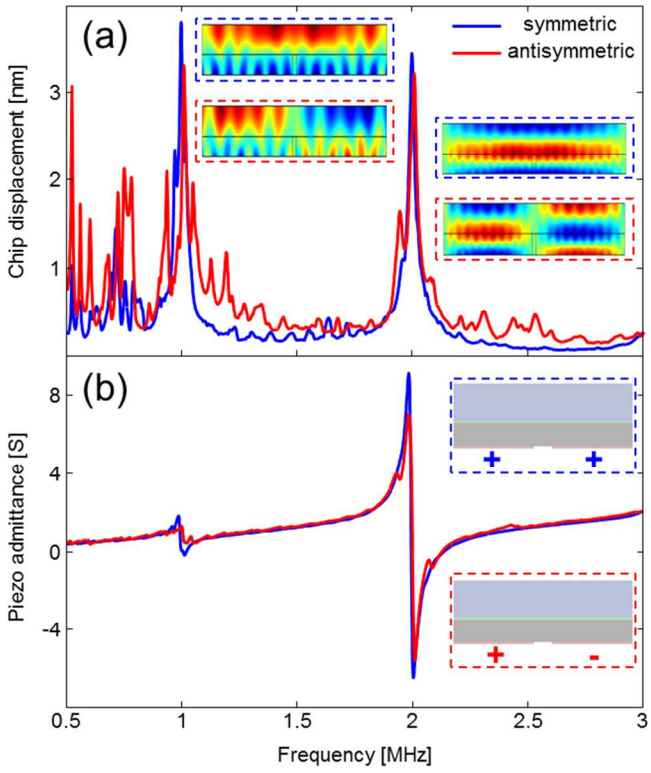

Fig. 5 Excitation of elastic waves in the glass chip by applying a sinusoidal wave across the piezoelectric element in the three-terminal configuration for both symmetric and antisymmetric modes; schematic inset in (b) shows voltage applied across piezoelectric transducer. Displacement amplitude (a) and admittance (b) are plotted as a function of frequency; the insets in (a) identify the first two transverse resonant modes of the system.

The modes of the bonded PZT-glass chip are calculated for transversal excitation (vertical electric field amplitude). Figure 5 presents the coupled elastic mode for a transducer-chip system for both symmetric and antisymmetric modes along with displacement amplitude (Euclidian norm, root mean square) and admittance spectrum for a transducer and chip of free frequency 1.99 MHz. For brevity displacement refers to maximum of root mean square displacement amplitude for all figures. The first and second modes of oscillation for the coupled system are identified in the displacement insets around 1 and 2 MHz. At lower frequencies (below 1 MHz) the amplitude spectrum also shows excitation of lateral modes. Further design of the acoustofluidic device aims to match the channel resonance with the 2 MHz mode. For the coupled system the symmetric mode occurs at 1.993 MHz and the antisymmetric mode at 2.002 MHz.

We also investigated the effect of frequency mismatch between the two components on the symmetric mode. For a given resonant frequency of the piezoelectric transducer of 2 MHz the free resonant frequency of the glass chip is adjusted by varying its thickness. The coupling efficiency is estimated by driving the piezoelectric element with a sinusoidal wave of amplitude 1V and plotting the frequency dependence of the maximum root mean square chip displacement and piezoelectric admittance for all considered thicknesses (Figure 6). The mode profile for mismatched piezo-chip frequencies (Figure 6.(a), inset) shows that the mode structure is the same as presented in Figure 6.(a), inset for matching piezo-chip frequencies. This finding indicates that from a design perspective the thickness of the piezoelectric transducer or that of the chip are not critical as long as the resonant frequency of the system matches the fluidic channel resonance. The amplitude of the chip oscillation does decrease when the frequency mismatch becomes larger, however for a broad range of chip thicknesses the chip amplitude is nearly constant the admittance spectrum exhibits maxima when the chip eigenfrequency is a multiple of the piezoelectric eigenfrequency (Figure 6, panel d) as the modes of the system more closely resemble the modes of the free piezoelectric transducer (Figures 3, 4). Importantly, a 1-D wave propagation model that assumes resonance when the full thickness of the device (piezoelectric transducer and chip) is a multiple of sound wavelengths would predict straight lines for the displacement maxima in Figure 6.(b), rather than the curving shapes observed here. This insight provides further evidence that coupled mode theory provides a more complete description of acoustofluidic device resonances, a conclusion that will have to be confirmed experimentally.

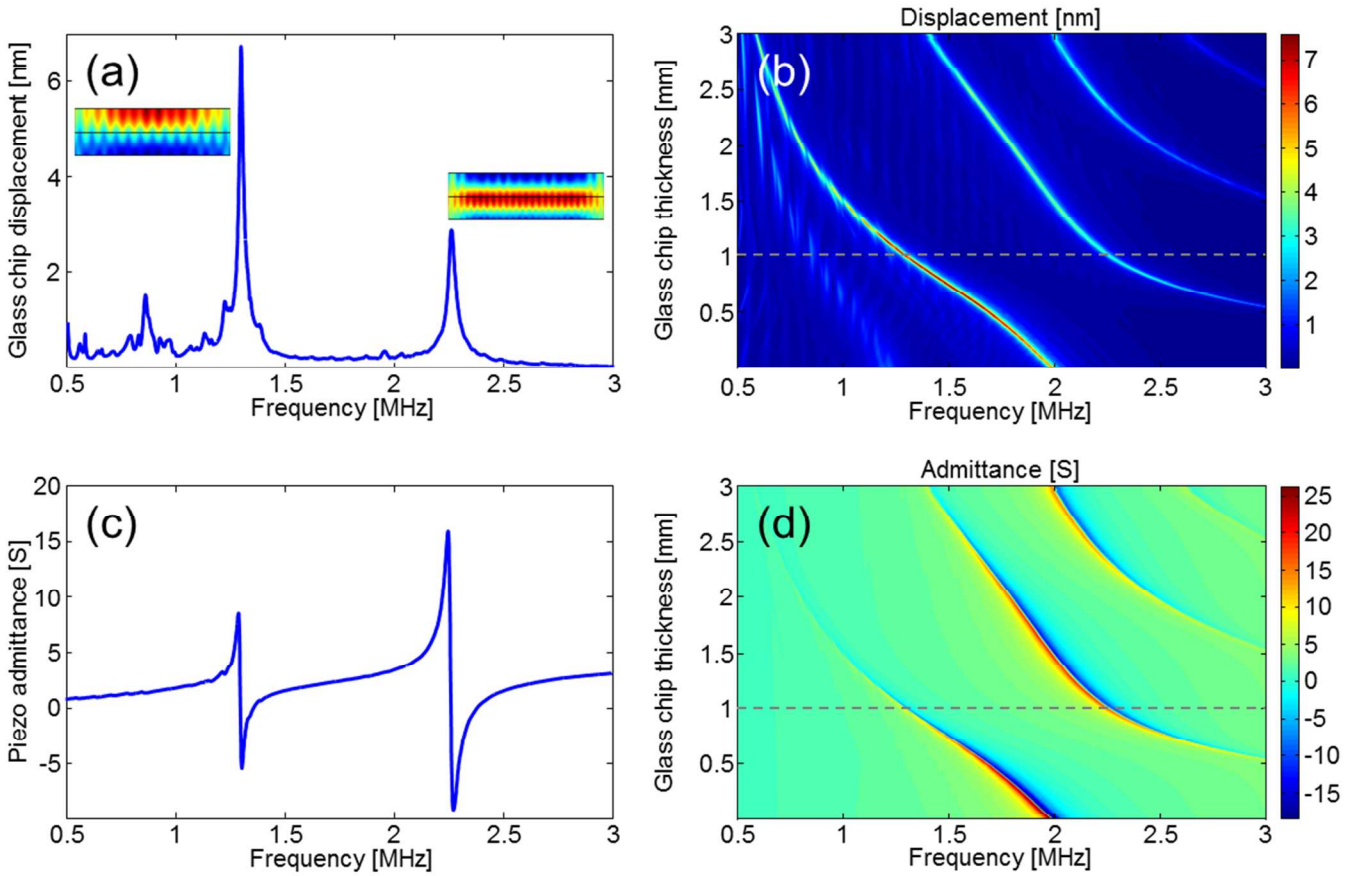

Fig. 6. Analysis of the mode frequency mismatch between the piezoelectric driver and glass chip. Displacement (a) and admittance spectrum (c) for a piezoelectric-glass chip system with free resonant frequencies at 2 MHz for the piezoelectric element and 2.99 MHz for the glass chip. The first two resonances of the combined system occur at 1.3 MHz and 2.3 Mhz. The inset in figure (a) shows the mode profile for each resonance. The displacement (b) and admittance (d) spectrum calculation is extended by varying the chip thickness. Dashed line in (b) and (d) corresponds to calculations plotted in (a) and (c).

Effects of channel cross section

The introduction of the fluidic channel in the chip influences the elastic modes due to addition of free movement boundaries around the channel. Added resonances are introduced for the elastic modes of subdivisions of the chip in regions directly below and above the channel. While it is possible to use these additional modes to excite the pressure wave in the channel, in practice it is more difficult to identify and characterize them using either admittance or vibrometry measurements. However, this remains an open route for improving the design considered in this paper.

In Figure 7 the displacement spectrum is calculated for a device with a channel cut-out cross section of 2 mm width and 0.1 mm height (chosen to match the 2 MHz chip-piezo resonant frequency with the channel empty, and free boundary conditions) placed in the centre of glass chip. The thicknesses of the glass and PZT transducer are 1.5 mm and 1.035 mm, and the width is the same for both at 25.4 mm. Two distinct oscillation modes are observed. The bulk mode (oscillations throughout the entire volume of the chip) is the second order transverse elastic mode at 2 MHz (Figure 7, right inset), and the localized mode, at 1.7 MHz, is a first-order transverse elastic mode arising in the device sub-section delimited by the free piezo interface and the bottom edge of the channel (Figure 7, left inset). The resonance of this localized mode shifts towards lower frequencies with increasing channel width. Additional localized modes can be excited in the glass section directly above the channel (not shown).

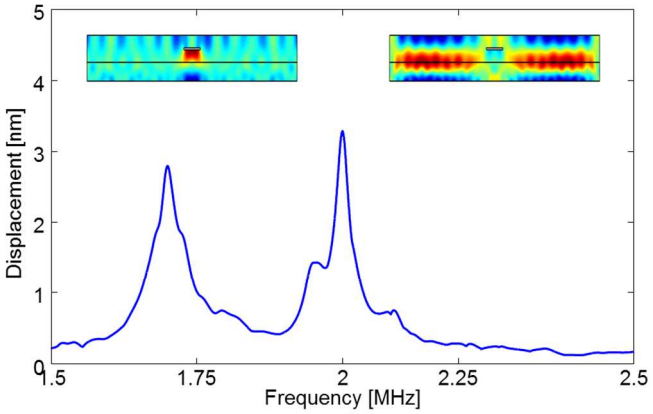

Fig. 7. Displacement spectrum for a piezoelectric chip device with fluidic channel. The insets show elastic modes for the bulk and localized resonances.

The bulk symmetric 2 MHz mode (Figure 7, right inset) shifts slightly towards lower frequencies (~10 kHz) with respect to the addition of the channel mainly due to a change is the total mass of the device.

Excitation of acoustic pressure modes in an integrated device: piezoelectric transducer, chip, fluidic channel

Having now built up the full geometry of the acoustofluidic device, it becomes possible to study its full functionality. The parameters that provide maximally-efficient energy transfer to the fluid are found by identifying the oscillation modes for the pressure in the fluidic channel and displacement in the piezoelectric driver and glass chip,.

The pressure amplitude in the microfluidic channel is maximized when the chip elastic frequency matches the acoustic frequency of the channel. This concept can be explained using a simple damped harmonic model[7] for the fluid channel of resonant frequency ω_0, driven by a force of amplitude F, and frequency ω. The coupling amplitude of a driven and damped harmonic oscillator has a Lorentzian form and is maximized when $\omega=\omega_0$. Alternatively, the frequency matching requirement can be understood from a mode theory perspective, which states that the coupling between two modes is proportional to their temporal and spatial overlap.

The coupling between the elastic modes of the chip and the acoustic modes in the channel is modelled using a solid-acoustic boundary condition:

$$n \cdot \frac{\nabla p}{\rho} = -n \cdot \frac{\partial^2 u}{\partial t^2}$$
$$s \cdot n = pn \qquad (12)$$

where the symbols are consistent with previous equations. Simply stated, the pressure gradient is proportional with the interface acceleration, and the pressure imposes a normal stress on the elastic material.

In Figure 8 the efficiency for excitation of ultrasound waves in the fluidic channel is compared for symmetric and anti-symmetric configurations for first- (Figure 8.a) and second-order (Figure 8.g) acoustic modes. Wall deformation and vertical displacement around the channel (Figure 8.b and 8.h) show that acoustic pressure maxima expand and pressure minimum contract the channel cross section. Structural elastic modes are presented in Figure 8.c and 8.i for the conditions that excite the highest pressure amplitude in the fluid. The behaviour of each component of the entire device is analysed by plotting the frequency dependence of admittance for the piezoelectric transducer (Figure 8.f and 8.l), displacement amplitude maximum for the glass chip (Figure 8.e and 8.k) and pressure maximum for the fluidic channel (Figure 8.d and 8.j) for both symmetric (blue) and antisymmetric (red) excitation of the piezoelectric element. The insets in Figure 8.d and 8.j show a schematic for symmetry of both drive signal and acoustic mode.

The simulation results indicate that symmetry matching is a required condition for optimal acoustic coupling efficiency. If the system modes are labelled by their positional symmetry for applied voltage (first index) and acoustic mode (second index) all four possible combinations are considered: ***aa***, ***as***, ***sa***, ***ss***. For example, the mode ***as*** is defined by $V_{(x)} = -V_{(-x)}$ and $p_{(x)} = p_{(-x)}$. Although the amplitude of admittance and chip displacement is approximately the same for all cases, the pressure amplitude has a strong dependence on symmetry matching throughout the device. Cross symmetric modes ***as***, ***sa*** have poor acoustic coupling, with ***sa*** mode relying on Poisson effect (i.e. deformation in the transverse direction of the chip, results in deformations in the lateral direction, Figure 8.d blue). Most efficient coupling is observed for identical symmetry device modes: ***aa***, and ***ss*** with pressure amplitudes at least one order of magnitude larger than cross-symmetric modes.

An additional consequence of this analysis is that the resonant frequencies of the fluidic channels calculated earlier using the hard wall approximation (Figure 3) are found to be inaccurate, since that approach did not consider the fluid-chip interaction. Acoustic resonances at 2 MHz occur for channel widths of 357 μm for the first mode and 714 μm for the second mode, compared to the hard wall approximation prediction of 375 μm and 750 μm. The glass chip and piezoelectric transducer width is 25.4 mm and thicknesses were 1.5 and 1.035 mm for Figures 8 and 9. Previous reports also show that elastic properties of chip material (silicon, glass[23], polymers[16], PDMS[30]) have strong effects on the acoustic modes in the fluid.

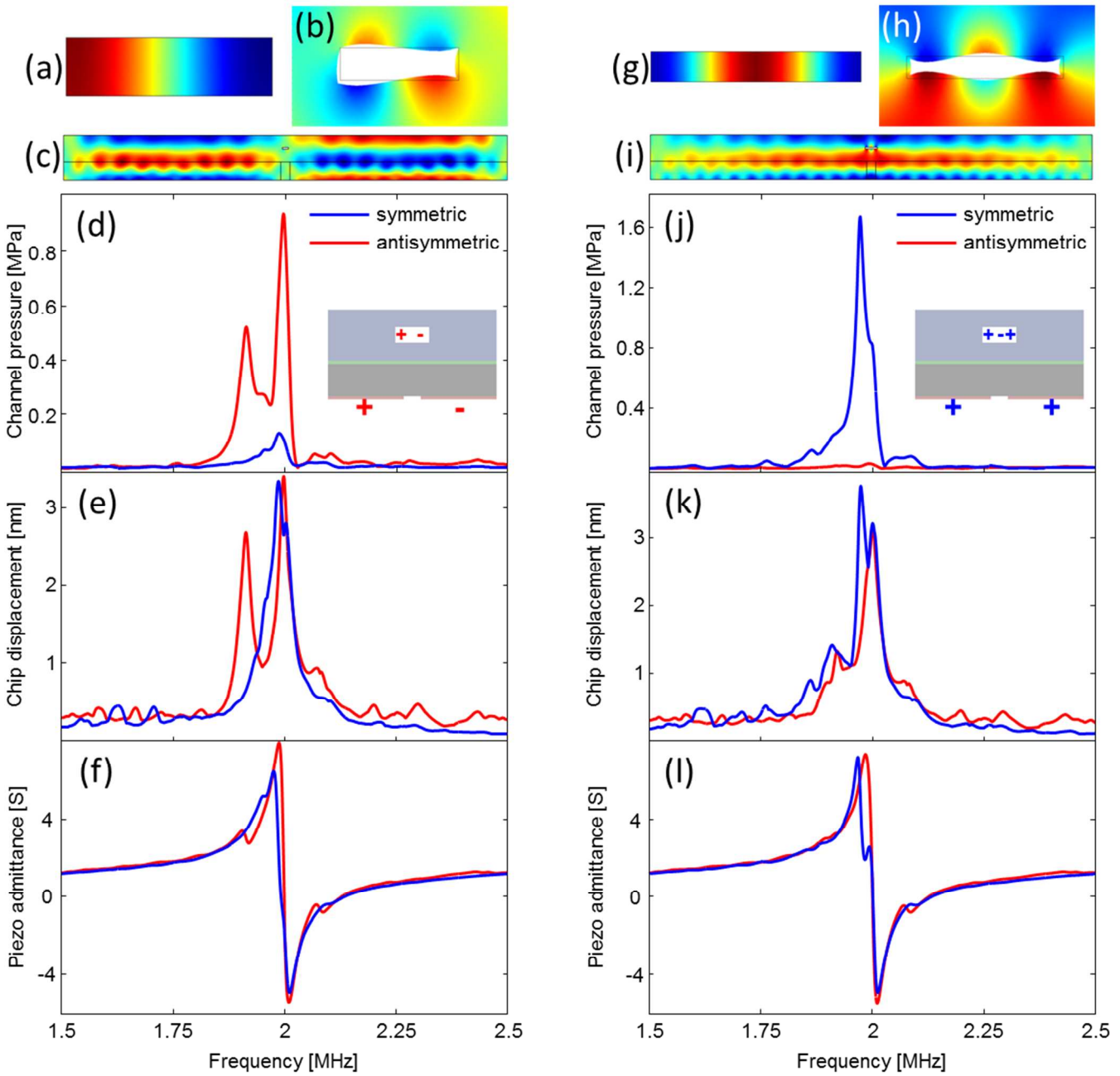

Fig. 8. Resonant modes for device designed to operate at the first (a) and second (g) acoustic modes. Fluidic channel wall vertical deformation (colour) and total deformation (contour) are plotted in b and h, along with vertical deformations in the piezo-chip device (c, i). Channel pressure amplitude in (d) and (j) show that maximum coupling take place when the piezoelectric actuation symmetry is the same as acoustic mode symmetry (inset d, j). Although there is no significant difference in glass chip oscillation amplitude (e, k) or piezoelectric admittance (f, l) symmetry matching increases the pressure amplitude by more than one order of magnitude.

Taking this approach further, the optimal channel cross section can now be determined by varying the channel width in a transversal elastic mode device and calculating the resulting acoustic pressure amplitude maximum (Figure 9). In this analysis, the piezoelectric element is driven in the symmetric mode. The result is a two dimensional mapping that allows estimation of acoustic coupling efficiency for arbitrary detuning between device and channel resonances (note that the pressure scale is logarithmic). As shown in previous calculations the elastic resonances occur approximately at 1, 2, and 3 MHz for first, second and third order transverse modes. Additional modes identified in Figure 7 arise at slightly lower frequencies and are localized in the vicinity of the channel. Channel resonant frequencies calculated using the hard wall approximation are superimposed for antisymmetric (red) and symmetric acoustic modes (blue). Since the piezoelectric transducer is driven in the symmetric configuration the odd acoustic modes are suppressed (***sa***), while the even acoustic modes are enhanced (***ss***). As observed when comparing Figure 8 to Figure 3, the hard wall approximation overestimates the actual resonant frequency of the channel as it does not account for wall deformations due to fluidic pressure.

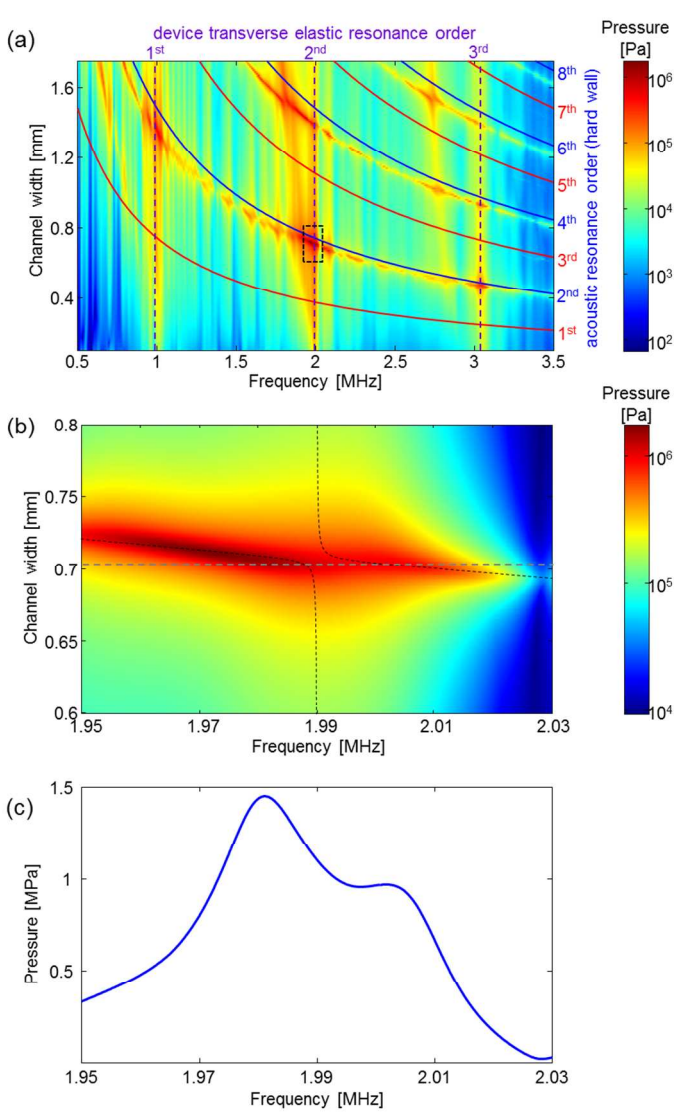

Fig. 9 Mapping of the acoustic coupling strength in the device. (a) Logarithmic plot of pressure amplitude in a symmetric actuation device with transverse elastic resonances at 1, 2, and 3 MHz. Hard wall approximation for all channel widths are plotted for symmetric (blue) and antisymmetric (red) acoustic modes. Strongest acoustic coupling occurs for symmetric channel modes with frequency that matches the transverse elastic mode. (b) High resolution plot of dashed black line box in (a) of the maximum pressure amplitude configuration (i.e. second order transverse elastic, second order acoustic). Dashed lines represent frequency crossing calculation from coupled mode theory. (c) Pressure amplitude as a function of frequency for a channel 0.704 mm wide, dashed grey line in (b), showing degeneracy lifting of the acoustic mode into two distinct peaks.

The landscape in Figure 9.a reveals that ultrasonic modes in the fluid can be excited for almost any channel width, in good agreement with a multitude of literature reports that detail operation of acoustophoretic devices fabricated without special concern for chip dimensions. This finding is explained by considering the size of acoustofluidic chips with typical ~10 mm-scale lateral dimensions. The lateral elastic modes in such devices are closely spaced (10-100 kHz) and sufficiently broadened by elastic losses that the condition of matching the channel acoustic resonance with any elastic mode in the device is almost always realized. The transverse elastic modes have larger frequency separation of roughly 1 MHz, but have the benefit of larger elastic

displacement amplitudes translating into notable increases in fluid acoustic pressure. The most efficient coupling is realized when the transverse elastic frequency matches the fluid acoustic frequency resulting in pressure amplitudes that are approximately ten to fifteen times larger compared to excitation through lateral modes, corresponding to a potential decrease in required power input over one order of magnitude. Coupled mode analysis of the interaction between fluid acoustic and chip elastic modes predicts observation of frequency crossing for the oscillation of the entire system (Figure 2). The characteristic anti-crossing effect of strong coupling regime leads to frequency splitting into two branches: symmetric (fluid pressure and wall deformation are in phase) and antisymmetric (fluid pressure and wall deformation are 180° out of phase)[31]. Indeed, the anti-crossing structure is observed for all acoustic resonances in Figure 9.a and is more noticeable for larger channel widths and localized subsection chip resonances for which the acoustic and elastic energies are comparable. Figure 9.b shows a higher resolution zoom-in of the maximal pressure mode corresponding to the frequency matching of the second order transverse elastic mode of the device and the second order acoustic mode in the channel. The overlaid dashed lines represent calculation of chip-channel resonant frequencies ν_S and ν_A based on coupled-mode theory from equation (4), with device frequency ν_1=1.99 MHz, and channel resonant frequency derived from cavity round trip phase change of multiple of 2π:

$$\upsilon_2 = \frac{mc}{2w} \qquad (13)$$

Where ***m*** is the resonance order, ***c*** is the speed of sound in water, and ***w*** is the width of the channel. The estimated coupling strength, ***k***, is 5 kHz, and the speed of sound in the channel 1407 m/s, compared to bulk speed of sound in water of 1481.4 m/s. The discrepancy between the two velocities originates in the fluid solid interaction resulting in an equivalent correction for sound wavelength[32]. The model predicts that for certain channel geometries two distinct focusing peaks arise, with small separation, on the order of 10s of kHz (Figure 9.c).

Discussion

In this numerical study of acoustofluidic resonator design, new insights were gained by applying coupled-mode theory for calculating the fluid-structure interaction. By considering a simple acoustic device architecture, consisting of a planar piezo transducer coupled to an all-glass chip containing a microfluidic channel, this approach was applied to find design rules to maximize energy transfer from the piezoelectric element into the acoustic mode. Two key design rules for acoustofluidic devices were identified from simple theoretical arguments: (1) frequency matching and (2) symmetry matching between the fluid cavity resonant modes and transducer-chip ensemble elastic mode.

In order to excite modes with specific symmetries we proposed a three-terminal piezo actuation scheme. One side is patterned with a single ground electrode and the opposite side is divided in half parallel to the channel length to allow symmetric and antisymmetric actuation. While another report[21] has predicted significant differences in acoustic pressure spectra resulting from various piezo actuation schemes, our work is the first detailed study of these effects, and the first effort to optimize acoustofluidic design parameters based on these considerations.

The proposed design has several advantages over alternative approaches. First, precision in selecting lateral chip dimensions (i.e. multiples of sound wavelength), as it relies solely on the transverse elastic mode. Second, for strongly bonded interfaces the thicknesses of different layers, transducer, coupler and reflector, are not critical as long as the combined piezo-chip structure has a transverse resonant frequency matching that of the acoustic channel.

It is important to account for resonance modes of subsections of the chip, such as the glass section directly above or below the channel that can give rise to beam-like vibrations depending on the thickness and length of that segment. These modes can enhance or suppress the desired acoustic resonance, based on similar arguments on frequency- and symmetry-matching presented in this paper. Exploiting these subsection resonances in an acoustofluidic device may prove difficult in practice, as tighter tolerances on chip dimensions would be required. A more rigorous analysis is needed to quantify the benefit of these features with respect to enhancing the acoustic field in the channel

We advocate using the bulk transverse resonances because they are straightforward to identify experimentally through admittance measurements both before and after attaching the transducer to the chip, providing valuable feedback on the elastic mode frequency. The simulation approach presented here can be improved by a more realistic simulation of the transducer-chip coupling layer, which was assumed to be "perfect" in this work (i.e. continuous displacement condition across the interface). We note that many previous reports[19, 33, 34] have matched the resonance of the free, unloaded piezo to the fluid cavity mode, without concern for the full piezo-chip structure. We infer that this can be attributed to "soft" piezo-chip coupling, which allows the piezo to vibrate independently of the fluidic chip. The energy transfer into the fluid is therefore highly inefficient, but this condition relaxes the requirement of full-structure resonance matching.

Finally, the all-glass design in this study was primarily intended to demonstrate the power of our approach, and to reduce the initial complexity of device modelling. The results from this work can be readily extended to more complex acoustic chips composed of different material layers.

Conclusions

In this work we propose a simple and robust architecture for acoustofluidic chips that follow two design rules. The first constraint is matching the transverse mode elastic frequency of the piezoelectric transducer chip ensemble to that of the acoustic channel. The second constraint is matching the symmetry of the actuation voltage on the piezoelectric transducer to the positional symmetry of pressure in the acoustic mode. The proposed design provides a path toward significant increases in achievable

acoustic pressure amplitude compared to existing devices, with potential benefits for more efficient particle manipulation.

Acknowledgements

This work was performed under the auspices of the U.S. Department of Energy by Lawrence Livermore National Laboratory under Contract DE-AC52-07NA27344. We thank Dr. Jack Kotovsky for his insightful comments on the manuscript. LLNL-JRNL-664577.

Notes and references

[a] Lawrence Livermore National Laboratory, 7000 East Ave., Livermore, CA 94550

E-mail: bora1@llnl.gov

1. P. Sajeesh and A. K. Sen, *Microfluidics and Nanofluidics*, 2014, 17, 1-52.
2. A. Lenshof and T. Laurell, *Chem. Soc. Rev.*, 2010, 39, 1203-1217.
3. T. Laurell, F. Petersson and A. Nilsson, *Chem. Soc. Rev.*, 2007, 36, 492-506.
4. Z. C. Wang and J. A. Zhe, *Lab Chip*, 2011, 11, 1280-1285.
5. J. Dual and D. Moller, *Lab Chip*, 2012, 12, 506-514.
6. J. Dual and T. Schwarz, *Lab Chip*, 2012, 12, 244-252.
7. H. Bruus, *Lab Chip*, 2012, 12, 20-28.
8. J. Nam, H. Lim, D. Kim and S. Shin, *Lab Chip*, 2011, 11, 3361-3364.
9. X. Ding, Z. Peng, S.-C. S. Lin, M. Geri, S. Li, P. Li, Y. Chen, M. Dao, S. Suresh and T. J. Huang, *Proceedings of the National Academy of Sciences of the United States of America*, 2014, 111, 12992-12997.
10. L. P. Gor'kov, *Sov. Phys. Dokl.*, 1962, 6.
11. K. Yosioka and Y. Kawasima, *Acustica*, 1955, 5, 167-173.
12. M. Settnes and H. Bruus, *Phys. Rev. E*, 2012, 85.
13. G. Goddard and G. Kaduchak, *J. Acoust. Soc. Am.*, 2005, 117, 3440-3447.
14. G. Goddard, J. C. Martin, S. W. Graves and G. Kaduchak, *Cytom. Part A*, 2006, 69A, 66-74.
15. M. Wiklund, S. Nilsson and H. M. Hertz, *J. Appl. Phys.*, 2001, 90, 421-426.
16. I. Gonzalez, L. J. Fernandez, T. E. Gomez, J. Berganzo, J. L. Soto and A. Carrato, *Sens. Actuator B-Chem.*, 2010, 144, 310-317.
17. J. Nilsson, M. Evander, B. Hammarstrom and T. Laurell, *Anal. Chim. Acta*, 2009, 649, 141-157.
18. A. Nilsson, F. Petersson, H. Jonsson and T. Laurell, *Lab Chip*, 2004, 4, 131-135.
19. R. Barnkob, P. Augustsson, T. Laurell and H. Bruus, *Lab Chip*, 2010, 10, 563-570.
20. A. Lenshof, M. Evander, T. Laurell and J. Nilsson, *Lab Chip*, 2012, 12, 684-695.
21. A. Neild, S. Oberti and J. Dual, *Sens. Actuator B-Chem.*, 2007, 121, 452-461.
22. O. Manneberg, J. Svennebring, H. M. Hertz and M. Wiklund, *J. Micromech. Microeng.*, 2008, 18.
23. M. Evander, A. Lenshof, T. Laurell and J. Nilsson, *Anal. Chem.*, 2008, 80, 5178-5185.
24. Y. Bellouard, A. Said, M. Dugan and P. Bado, *Opt. Express*, 2004, 12, 2120-2129.
25. A. Marcinkevicius, S. Juodkazis, M. Watanabe, M. Miwa, S. Matsuo, H. Misawa and J. Nishii, *Opt. Lett.*, 2001, 26, 277-279.
26. H. A. Haus and W. P. Huang, *Proc. IEEE*, 1991, 79, 1505-1518.
27. W. P. Huang, *J. Opt. Soc. Am. A-Opt. Image Sci. Vis.*, 1994, 11, 963-983.
28. D. E. Newland, *J. Sound Vibr.*, 1966, 3, 262-&.
29. T. D. Rossing and D. A. Russell, *American Journal of Physics*, 1990, 58, 1153-1162.
30. N. Leibacher, S. Schatzer and J. Dual, *Lab Chip*, 2014, 14, 463-470.
31. L. Novotny, *American Journal of Physics*, 2010, 78, 1199-1202.
32. R. Barnkob and H. Bruus, *Proceedings of Meetings on Acoustics*, 2009, 6.
33. F. Petersson, A. Nilsson, H. Jonsson and T. Laurell, *Anal. Chem.*, 2005, 77, 1216-1221.
34. O. Manneberg, S. M. Hagsater, J. Svennebring, H. M. Hertz, J. P. Kutter, H. Bruus and M. Wiklund, *Ultrasonics*, 2009, 49, 112-119.

